Supplementary Information for "Alternating twisted multilayer graphene: generic partition rules, double flat bands, and orbital magnetoelectric effect"

Bo Xie,[1] Ran Peng,[1] Shihao Zhang,[1] and Jianpeng Liu[1,2,*]

[1]*School of Physical Science and Technology, ShanghaiTech University, Shanghai 201210, China*
[2]*ShanghaiTech laboratory for topological physics, ShanghaiTech University, Shanghai 201210, China*

(Dated: April 6, 2022)

I. SUPPLEMENTARY METHODS

A. Details of the continuum Hamiltonian

The low-energy electronic structure of ATMG can be well described based on the Bistritzer-MacDonald continuum model[1]. The continuum model describing the $\mu = \mp$ valley is:

$$H^{\mu}_{ATMG} = \begin{pmatrix} H^{\mu}_{N} & \mathbb{U}^{\dagger}_{\mu} e^{-i\mu\Delta\mathbf{K}\cdot\mathbf{r}} & 0 \\ \mathbb{U}_{\mu} e^{i\mu\Delta\mathbf{K}\cdot\mathbf{r}} & H^{\mu}_{L} & \mathbb{U}_{\mu} e^{i\mu\Delta\mathbf{K}\cdot\mathbf{r}} \\ 0 & \mathbb{U}^{\dagger}_{\mu} e^{-i\mu\Delta\mathbf{K}\cdot\mathbf{r}} & H^{\mu}_{M} \end{pmatrix} \tag{1}$$

where H^{μ}_{N}, H^{μ}_{L} and H^{μ}_{M} denote the $\mathbf{k}\cdot\mathbf{p}$ Hamiltonians of the untwisted graphene multilayers, which consist of the Dirac fermions of each monolayer graphene and the interlayer hopping terms. $\mathbb{U}_{\mu} e^{i\mu\Delta\mathbf{K}\cdot\mathbf{r}}$ stands for the moiré potential term for valley μ, which arises from the mutual twist between two sets of adjacent multilayers. $\Delta\mathbf{K} = (0, 4\pi/(3L_s))$ is a vector characterizing the shift of Dirac points due to the twist.

$$H^{\mu}_{M} = \begin{pmatrix} h^{\mu}_{0}(\mathbf{k}) & h_{\alpha} & 0 & 0 & \cdots \\ h^{\dagger}_{\alpha} & h^{\mu}_{0}(\mathbf{k}) & h_{\alpha} & 0 & \cdots \\ 0 & h^{\dagger}_{\alpha} & h^{\mu}_{0}(\mathbf{k}) & h_{\alpha} & \cdots \\ & & & \cdots & \end{pmatrix} \tag{2}$$

where $h^{\mu}_{0}(\mathbf{k}) = -\hbar v_F(\mathbf{k} - \mathbf{K}_M)\cdot\boldsymbol{\sigma}^{\mu}$, $\boldsymbol{\sigma}^{\mu} = (\mu\sigma_x, \sigma_y)$. Here we only consider interlayer hopping for two adjacent layers. h_{α} is the interlayer hopping matrix for different stacking chirality α, where $\alpha, \alpha' = +, -$, and $h_{-} = h^{\dagger}_{+}$. If we only consider nearest neighbor hopping, the hopping matrix is:

$$h_{+} = \begin{pmatrix} 0 & 0 \\ t_{\perp} & 0 \end{pmatrix} \tag{3}$$

Taking further neighbor hopping for untwisted layers into account, the flat bands will be more dispersive. The hopping matrix is:

$$h_{+} = \begin{pmatrix} t_2 f(\mathbf{k}) & t_2 f^{*}(k) \\ t_{\perp} - 3t_3 & t_2 f(\mathbf{k}) \end{pmatrix}. \tag{4}$$

We set $t_{\perp}$=0.48eV, t_2=0.21eV,t_3=0.05eV. The phase factor is $f(\mathbf{k}) = e^{-i\sqrt{3}k_y a/3} + e^{i(k_x a/2 + \sqrt{6}k_y a/6)} + e^{i(-k_x a/2 + \sqrt{3}k_y a/6)}$ [2].

$\mathbb{U}$ is the interlayer hopping between two adjacent sequences of multilayers:

$$\mathbb{U} e^{-i\Delta\mathbf{K}\cdot\mathbf{r}} = \begin{pmatrix} 0 & \cdots & 0 \\ \vdots & \cdots & \vdots \\ U(\mathbf{r}) e^{-i\Delta\mathbf{K}\cdot\mathbf{r}} & \cdots & 0 \end{pmatrix}. \tag{5}$$

*liujp@shanghaitech.edu.cn

where $U(\mathbf{r})$ describes the interlayer hopping induced by moiré pattern:

$$U(\mathbf{r}) = \begin{pmatrix} u_0 g(\mathbf{r}) & u_0' g(\mathbf{r}-\mathbf{r}_{AB}) \\ u_0' g(\mathbf{r}+\mathbf{r}_{AB}) & u_0 g(\mathbf{r}) \end{pmatrix} \tag{6}$$

with $u_0 = 0.0797\,\text{eV}$, $u_0' = 0.0975\,\text{eV}$, $\mathbf{r}_{AB} = (\sqrt{3}L_s/3, 0)$. Because of the corrugation effects, the intrasublattice term u_0 is different from the intersublattice term u_0'[3]. The phase factor is defined as $g(\mathbf{r}) = \sum_{j=1}^{3} e^{i\mathbf{q}_j\cdot\mathbf{r}}$, and $\mathbf{q}_1 = (0, 2/3)\cdot 2\pi/L_s$, $\mathbf{q}_2 = (-1/\sqrt{3}, -1/3)\cdot 2\pi/L_s$ and $\mathbf{q}_1 = (1/\sqrt{3}, -1/3)\cdot 2\pi/L_s$. $\Delta\mathbf{K} = \mathbf{K}_2 - \mathbf{K}_1 = (0, 2/3)\cdot 2\pi/L_s$ is the shift between Dirac fermion from two twisted layers.

For any ATMG system with $L=1$, we can apply the unitary transformation given by Eq. (8) of main text to the three alternating twisted layers, and keep other layers unchanged. The corresponding layer-mixed basis functions are: $\bar{\psi}^{\mu}_{\alpha s,\mathbf{k}}(\mathbf{r}) = \widetilde{\psi}^{\mu}_{Ls,\mathbf{k}}(\mathbf{r}), \bar{\psi}^{\mu}_{\beta s,\mathbf{k}}(\mathbf{r}) = \frac{-1}{\sqrt{2}}\widetilde{\psi}^{\mu}_{Ms,\mathbf{k}}(\mathbf{r}) + \frac{1}{\sqrt{2}}\widetilde{\psi}^{\mu}_{Ns,\mathbf{k}}(\mathbf{r}), \bar{\psi}^{\mu}_{\gamma s,\mathbf{k}}(\mathbf{r}) = \frac{1}{\sqrt{2}}\widetilde{\psi}^{\mu}_{Ms,\mathbf{k}}(\mathbf{r}) + \frac{1}{\sqrt{2}}\widetilde{\psi}^{\mu}_{Ns,\mathbf{k}}(\mathbf{r})$, where α, β, γ are the three mix-layer indices marking the basis functions after the unitary transformation, $\widetilde{\psi}^{\mu}_{ls,\mathbf{k}}(\mathbf{r})$ with $l = M, L, N$ denote the basis wave functions (after the gauge transformation) of the three alternating twisted layers in the M, L, and N sequence respectively, and $s = A, B$ is the sublattice index. After such a transformation, the continuum Hamiltonian consists of a TBG-like part and a free Dirac fermion (as shown in Eq. (7) of main text) contributed by the three alternating twisted layers, with the terms from the other layers being unchanged. One can solve for the zero-mode solutions for the TBG-like part at the renormalized magic angle $\sqrt{2}\times 1.05^\circ$, and expand all the Dirac cones around the Dirac points within the moiré Brillouin zone, then eventually obtain a $\mathbf{k}\cdot\mathbf{p}$ model in a greatly simplified form. For L>1, above transformation is unnecessary, since there are two pairs of twisted layers giving rise to two TBG-like terms. For each of the TBG-like terms, we can obtain the zero-mode solution of magic-angle TBG in the chiral limit. We construct simplified $\mathbf{k}\cdot\mathbf{p}$ model to describe the low-energy dispersion of ATMG systems.

B. Examples of simplified $\mathbf{k}\cdot\mathbf{p}$ model

We take the *AB-A-AB* and *AB-A-BA* stacked ATMG systems as two typical examples to illustrate how the partition rule works. Following the procedures described above, we obtain the simplified $\mathbf{k}\cdot\mathbf{p}$ Hamiltonian for *AB-A-AB* (*AB-A-BA*) stacked ATMG system:

$$H^{\mathbf{k}\cdot\mathbf{p}} = \begin{pmatrix} h(\mathbf{k}) & \tilde{h}_+ & -h_+ & \tilde{h}_+ & 0 \\ \tilde{h}_+ & 0 & 0 & 0 & \tilde{h}_{+(-)} \\ -h_- & 0 & h(\mathbf{k}) & 0 & h_{+(-)} \\ \tilde{h}_- & 0 & 0 & 0 & \tilde{h}_{+(-)} \\ 0 & \tilde{h}_{+(-)} & h_{+(-)} & \tilde{h}_{+(-)} & h(\mathbf{k}) \end{pmatrix}, \tag{7}$$

where

$$h_+ = \begin{pmatrix} 0 & 0 \\ t_\perp & 0 \end{pmatrix}, \tilde{h}_+ = \begin{pmatrix} 0 & 0 \\ \tilde{t}_\perp & 0 \end{pmatrix} \tag{8}$$

$h(\mathbf{k}) = -\hbar v_F \mathbf{k}\cdot\boldsymbol{\sigma}$, and $h_- = h_+^\dagger$ for different stacking chirality. The "+(−)" sign in $\tilde{h}_{+(-)}$ in Eq. (7) applies to the *AB-A-AB* (*AB-A-BA*) stacking. $t_\perp$ is the interlayer intersublattice hopping parameter. In the chiral limit we only consider nearest neighbor interlayer hopping term, and $\tilde{t}_\perp$ is the renormalized hopping parameter.

Then we provide the expression of $\tilde{h}_+$ in Eq. 8. Since we only consider the nearest neighbor hopping term in the chiral limit, the interlayer hopping matrix would couple the A(B) sublattice of one layer and B(A) sublattice. For coupling between Dirac fermion of top monolayer graphene and the zero modes from alternating twisted layers, the Dirac fermion from A(B) sublattice is coupled to two wave functions from B(A) sublattice. To be specific, we first consider the coupling between the Bloch state spinor in topmost layer (denoted as $\begin{pmatrix} u^*_{t,A}(\mathbf{r})e^{-i\mathbf{K}_1\cdot\mathbf{r}} & u^*_{t,B}(\mathbf{r})e^{-i\mathbf{K}_1\cdot\mathbf{r}} \end{pmatrix}^\dagger$) and the zero modes wave function $\begin{pmatrix} \Psi^*_{\alpha s,\mathbf{k}}(\mathbf{r}) & \Psi^*_{\gamma s,\mathbf{k}}(\mathbf{r}) \end{pmatrix}^\dagger$, where $s = A, B$ is the sublattice indices. The renormalized

hopping matrix between $u_{t,s}(\mathbf{r})e^{i\mathbf{K}_1\cdot\mathbf{r}}$ and $\Psi_{ls,\mathbf{k}}(\mathbf{r})$, is expressed as:

$$\begin{aligned}
\tilde{h}^t_{+,ss'} =& \begin{pmatrix} u_{t,s}(\mathbf{r})e^{i\mathbf{K}_1\cdot\mathbf{r}} \\ 0 \\ 0 \\ 0 \\ 0 \end{pmatrix}^\dagger \begin{pmatrix} 0 & 0 & h_+ & h_+ & 0 \\ 0 & 0 & 0 & 0 & 0 \\ h_- & 0 & 0 & 0 & h_{+(-)} \\ h_- & 0 & 0 & 0 & h_{+(-)} \\ 0 & 0 & h_{-(+)} & h_{-(+)} & 0 \end{pmatrix} \begin{pmatrix} 0 \\ \Psi_{\alpha s',\mathbf{k}}(\mathbf{r}) \\ 0 \\ \Psi_{\gamma s',\mathbf{k}}(\mathbf{r}) \\ 0 \end{pmatrix} \\
=& \int d\mathbf{r}\ u^*_{t,s}(\mathbf{r})e^{-i\mathbf{K}_1\cdot\mathbf{r}}h_+\Psi_{\gamma s',\mathbf{k}}(\mathbf{r}) \\
=& \int d\mathbf{r}\ u^*_{t,s}(\mathbf{r})e^{-i\mathbf{K}_1\cdot\mathbf{r}}h_+(\frac{1}{\sqrt{2}}\Psi_{Ns',\mathbf{k}}(\mathbf{r}) + \frac{1}{\sqrt{2}}\Psi_{Ms',\mathbf{k}}(\mathbf{r})) \\
=& \frac{1}{\sqrt{2}}\int d\mathbf{r}\ u^*_{t,s}(\mathbf{r})e^{-i\mathbf{K}_1\cdot\mathbf{r}}t_\perp\Psi_{Ns',\mathbf{k}}(\mathbf{r})\delta_{s,B}\delta_{s',A} \\
=& \frac{1}{\sqrt{2}}\tilde{t}_\perp\delta_{s,B}\delta_{s',A}
\end{aligned} \tag{9}$$

where $t_\perp$ is the interlayer intersublattice hopping parameter between two Dirac fermions. We decompose the zero modes wave function into layer basis. Since we only consider the interlayer hopping between adjacent layers, there is zero overlap between states in topmost layer and zero modes solution in M sequence. The coupling between the zero modes wave function and states from the bottom-most layer can be evaluated in a similar way:

$$\tilde{h}^b_{+,ss'} = \begin{pmatrix} 0 \\ \Psi_{\alpha s,\mathbf{k}}(\mathbf{r}) \\ 0 \\ \Psi_{\gamma s,\mathbf{k}}(\mathbf{r}) \\ 0 \end{pmatrix}^\dagger \begin{pmatrix} 0 & 0 & h_+ & h_+ & 0 \\ 0 & 0 & 0 & 0 & 0 \\ h_- & 0 & 0 & 0 & h_+ \\ h_- & 0 & 0 & 0 & h_+ \\ 0 & 0 & h_- & h_- & 0 \end{pmatrix} \begin{pmatrix} 0 \\ 0 \\ 0 \\ 0 \\ u_{b,s'}(\mathbf{r})e^{i\mathbf{K}_1\cdot\mathbf{r}} \end{pmatrix} = \frac{1}{\sqrt{2}}\tilde{t}_\perp\delta_{s,B}\delta_{s',A} \tag{10}$$

The explicit expressions of zero modes spinor from two sublattice are[4]:

$$\begin{aligned}
\Psi_{lA,\mathbf{k}}(\mathbf{r}) &= \frac{\vartheta_{(\mathbf{ka}_1/2\pi)-\frac{1}{6},\frac{1}{6}-(\mathbf{ka}_2/2\pi)}((x+iy)/(a_{2,x}+ia_{2,y}) \mid e^{i2\pi/3})}{\vartheta_{-\frac{1}{6},\frac{1}{6}}((x+iy)/(a_{1,x}+ia_{1,y}) \mid e^{i2\pi/3})} \begin{pmatrix} \bar{\psi}_{\alpha A\mathbf{K}}(\mathbf{r}) \\ \bar{\psi}_{\gamma A\mathbf{K}}(\mathbf{r}) \end{pmatrix}, \\
\Psi_{lB,\mathbf{k}}(\mathbf{r}) &= \frac{\vartheta^*_{(\mathbf{ka}_1/2\pi)-\frac{1}{6},\frac{1}{6}-(\mathbf{ka}_2/2\pi)}((-x-iy)/(a_{2,x}+ia_{2,y}) \mid e^{i2\pi/3})}{\vartheta^*_{-\frac{1}{6},\frac{1}{6}}((-x-iy)/(a_{1,x}+ia_{1,y}) \mid e^{i2\pi/3})} \begin{pmatrix} \bar{\psi}_{\alpha B\mathbf{K}}(\mathbf{r}) \\ \bar{\psi}_{\gamma B\mathbf{K}}(\mathbf{r}) \end{pmatrix},
\end{aligned} \tag{11}$$

where $l = \alpha, \gamma$, $\vartheta_{a,b}(x+iy \mid \tau) = \sum_{n=-\infty}^{\infty} e^{i\pi\tau(n+a)^2}e^{2\pi i(n+a)(n+b)}$, $\mathbf{a}_1, \mathbf{a}_2$ are the moiré supercell lattice vector.

Another intriguing band dispersion in ATMG is double flat bands. To illustrate the origin of the double flat bands, we first study two ATMG systems for $L=3$ with A-ABA-A (with double flat bands) and A-ABC-A (with one pair of flat bands) stacking based on the simplified $\mathbf{k}\cdot\mathbf{p}$ model. To be specific, the simplified $\mathbf{k}\cdot\mathbf{p}$ Hamiltonian of the A-ABA-A system can be written as a direct sum of a 6×6 matrix and two zero modes

$$H^{\mathbf{k}\cdot\mathbf{p}}_{A-ABA-A} = \begin{pmatrix} 0 & \tilde{h}_+ & 0 \\ \tilde{h}_- & h(\mathbf{k}) & \tilde{h}_- \\ 0 & \tilde{h}_+ & 0 \end{pmatrix} \oplus \begin{pmatrix} 0 & 0 \\ 0 & 0 \end{pmatrix}, \tag{12}$$

where the 6×6 matrix consists of two zero modes coupled with a free Dirac fermion. Then it is straightforward to check that the eigenvalues of this 6×6 matrix has two zero modes, so that the entire system has four zero modes, leading to double flat bands. For A-ABC-A, the simplified $\mathbf{k}\cdot\mathbf{p}$ model can be written in a similar form

$$H_{A-ABC-A} = \begin{pmatrix} 0 & \tilde{h}_+ & 0 \\ \tilde{h}_- & h(\mathbf{k}) & \tilde{h}_+ \\ 0 & \tilde{h}_- & 0 \end{pmatrix} \oplus \begin{pmatrix} 0 & 0 \\ 0 & 0 \end{pmatrix} \tag{13}$$

Due to the change of stacking chirality, the 6×6 Hamiltonian consisting of two zero modes coupled with a free Dirac fermion no longer has zero-mode solution. Thus, there are only two zero modes for the A-ABC-A system, contributing to one pair of flat bands per spin per valley.

We can generalize the above argument for $L > 3$ and $M, N > 1$. According to the partition rules, the number of chiral segments in the L multilayers have a dramatic influence on the number of flat bands, while the segments in the

M and N multilayers do not. First, if the middle L multilayers has a chiral stacking, i.e., $S_L=1$, then the system is equivalent to the A-ABC-A system with a renormalized interlayer hopping parameter between untwisted layers $t'_\perp$. As a result, there is only one pair of flat bands (in the chiral limit) for the middle L layers with chiral stacking. Second, if the L multilayers can be decomposed into two segments($S_L=2$), the corresponding simplified $\mathbf{k}\cdot\mathbf{p}$ model is equivalent to that of the A-ABA-A system with renormalized hopping parameters, which has double flat bands. Finally, for $S_L>2$: we can argue that for alternating twist multilayers, two pairs of moiré potentials are coupled together through several chiral segments within the L multilayers, so that the more the segments are, the weaker the couple is. As a result, we can treat them as nearly decoupled and there are four flat bands for the $S_L>2$ situation. Therefore, if the middle L multilayers has $S_L>1$, there would be double flat bands for each spin and valley degrees of freedom.

C. Coulomb interactions in twisted graphene systems

We consider the Coulomb interaction in real space in graphene system:

$$H_C=\frac{1}{2}\sum_{ii'jj'}\sum_{\alpha\alpha'\beta\beta'}\sum_{\sigma\sigma'}\hat{c}^\dagger_{i\alpha\sigma}\hat{c}^\dagger_{i'\alpha'\sigma'}U^{\alpha\beta\sigma,\alpha'\beta'\sigma'}_{ij,i'j'}\hat{c}_{j'\beta'\sigma'}\hat{c}_{j\beta\sigma}\ , \tag{14}$$

where i,j is the lattice vector, α,β is the sublattice, σ is spin.

$$\begin{aligned}U^{\alpha\beta\sigma,\alpha'\beta'\sigma'}_{ij,i'j'}=&\int d\mathbf{r}\,d\mathbf{r}'\,\frac{e^2}{4\pi\epsilon|\mathbf{r}-\mathbf{r}'|}\,\phi^*_\alpha(\mathbf{r}-\mathbf{R}_i-\tau_\alpha)\,\phi_\beta(\mathbf{r}-\mathbf{R}_j-\tau_\beta)\\&\times\phi^*_{\alpha'}(\mathbf{r}-\mathbf{R}'_i-\tau_{\alpha'})\phi_{\beta'}(\mathbf{r}-\mathbf{R}'_j-\tau_{\beta'})\chi^\dagger_\sigma\chi^\dagger_{\sigma'}\chi_{\sigma'}\chi_\sigma\ .\end{aligned} \tag{15}$$

$U^{\alpha\beta\sigma,\alpha'\beta'\sigma'}_{ij,i'j'}$ describes the interaction between two electrons: the first one with spin σ is created at α sublattice with lattice vector i and annihilated at β sublattice with lattice vector j; the second electron with spin σ' is created at α' sublattice with lattice vector i' and annihilated at β' sublattice with lattice vector j'. Here we only keep dominant 'density-density' like interaction term in the system. We can separate the Coulomb interaction into inter-site and on-site term. Since the charge density is quite low in moiré super cell for electrons from flat bands, we can neglect on-site Hubbard interaction. We take Fourier transformation to the real space electron field operator:

$$\hat{c}_{i\alpha\sigma}=\frac{1}{\sqrt{N_s}}\sum_{\mathbf{k}_a}e^{i\mathbf{k}\cdot\mathbf{R}_i}\hat{c}_{\mathbf{k}_a\alpha\sigma} \tag{16}$$

$\mathbf{k}_a$ is the wave vector in atomic Brillouin zone, N_s is the number of atomic unit cell. We can expand the low energy states for twisted graphene around the atomic wave vector, i.e. $\mathbf{k}_a=\mathbf{k}+\mathbf{K}$, where $\mathbf{k}$ is the wave vector in moiré Brillouin zone, $\mathbf{K}$ is the moiré reciprocal lattice vector. Then the inter-site Coulomb interaction can be divided into inter-valley term and intravalley term[5]:

$$\begin{aligned}H_C^{\text{intra}}&=\frac{1}{2N_s}\sum_{\alpha\alpha'}\sum_{\mu\mu',\sigma\sigma'}\sum_{\mathbf{k}_a\mathbf{k}'_a\mathbf{q}_a}V(\mathbf{q}_a)\,\hat{c}^\dagger_{\mathbf{k}_a+\mathbf{q}_a,\mu\sigma\alpha}\hat{c}^\dagger_{\mathbf{k}'_a-\mathbf{q}_a,\mu'\sigma'\alpha'}\,\hat{c}_{\mathbf{k}'_a,\mu'\sigma'\alpha'}\hat{c}_{\mathbf{k}_a,\mu\sigma\alpha}\ ,\\H_C^{\text{inter}}&=\frac{1}{2N_s}\sum_{\alpha\alpha'}\sum_{\mu,\sigma\sigma'}\sum_{\mathbf{k}_a\mathbf{k}'_a\mathbf{q}_a}V(|\mathbf{K}-\mathbf{K}'|)\,\hat{c}^\dagger_{\mathbf{k}_a+\mathbf{q}_a,\mu\sigma\alpha}\hat{c}^\dagger_{\mathbf{k}'_a-\mathbf{q}_a,-\mu\sigma'\alpha'}\hat{c}_{\mathbf{k}'_a,\mu\sigma'\alpha'}\hat{c}_{\mathbf{k}_a,-\mu\sigma\alpha}\ .\end{aligned} \tag{17}$$

To reach a realistic situation, we consider the screening effect from the device: the single-gate screened Coulomb interaction is $V(\mathbf{q}_a)=e^2(1-e^{-2*|\mathbf{q}_a|d_s})/(2\Omega_M\epsilon_{\text{BN}}|\mathbf{q}_a|)$, where Ω_M is the area of moiré unit cell, $d_s=400\,\text{Å}$ is the distance between graphene and gate and ϵ_{BN} is the dielectric constant of h-BN. We can evaluate the energy scale intervalley and intravalley Coulomb interaction: the typical intravalley interaction energy $V_M\approx 25\,\text{meV}$ for $\theta\approx 1.2°$, while the intervalley interaction energy $V(|\,\mathbf{K}-\mathbf{K}'\,|)\sim 0.35\,\text{meV}$ for $\theta\approx 1.2°$. As a result, we only consider intravalley Coulomb interaction in our calculation.

We can project the interaction from origin basis to band basis through:

$$\hat{c}_{\mathbf{k}_a,\mu\alpha\sigma}=\sum_n C_{\mu\alpha\mathbf{G},n}(\mathbf{k})\hat{c}_{\mu\sigma,n\mathbf{k}} \tag{18}$$

where $C_{\mu\alpha\mathbf{G},n}(\mathbf{k})$ is the expansion coefficient in the n-th Bloch eigenstate at moiré wave vector near valley μ. We can rewrite the intravalley interaction by applying above transformation:

$$H^{\text{intra}} = \frac{1}{2N_s}\sum_{\mathbf{k}\mathbf{k}'\mathbf{q}}\sum_{\substack{\mu\mu'\\\sigma\sigma'}}\sum_{\substack{nm\\n'm'}}\left(\sum_{\mathbf{Q}} V(\mathbf{Q}+\mathbf{q})\,\Omega^{\mu\sigma,\mu'\sigma'}_{nm,n'm'}(\mathbf{k},\mathbf{k}',\mathbf{q},\mathbf{Q})\right)\hat{c}^{\dagger}_{\mu\sigma,n\mathbf{k}+\mathbf{q}}\hat{c}^{\dagger}_{\mu'\sigma',n'\mathbf{k}'-\mathbf{q}}\,\hat{c}_{\mu'\sigma',m'\mathbf{k}'}\,\hat{c}_{\mu\sigma,m\mathbf{k}} \tag{19}$$

where $\Omega^{\mu\sigma,\mu'\sigma'}_{nm,n'm'}$ is:

$$\Omega^{\mu\sigma,\mu'\sigma'}_{nm,n'm'}(\mathbf{k},\mathbf{k}',\mathbf{q},\mathbf{Q}) = \sum_{\alpha\alpha'\mathbf{G}\mathbf{G}'} C^{*}_{\mu\sigma\alpha\mathbf{G}+\mathbf{Q},n}(\mathbf{k}+\mathbf{q})C^{*}_{\mu'\sigma'\alpha'\mathbf{G}'-\mathbf{Q},n'}(\mathbf{k}'-\mathbf{q})C_{\mu'\sigma'\alpha'\mathbf{G}',m'}(\mathbf{k}')C_{\mu\sigma\alpha\mathbf{G},m}(\mathbf{k}) \tag{20}$$

We can make Hartree-Fock approximation to the intersite intravalley Coulomb interaction so that the two-particle interaction can be solved in a mean-field single particle Hamiltonian. The Hartree term is:

$$\begin{aligned} H^{\text{intra}}_{H} =& \frac{1}{2N_s}\sum_{\mathbf{k}\mathbf{k}'}\sum_{\substack{\mu\mu'\\\sigma\sigma'}}\sum_{\substack{nm\\n'm'}}\left(\sum_{\mathbf{Q}} V(\mathbf{Q})\Omega^{\mu\sigma,\mu'\sigma'}_{nm,n'm'}(\mathbf{k},\mathbf{k}',0,\mathbf{Q})\right) \\ &\times\left(\langle\hat{c}^{\dagger}_{\mu\sigma,n\mathbf{k}}\hat{c}_{\mu\sigma,m\mathbf{k}}\rangle\hat{c}^{\dagger}_{\mu'\sigma',n'\mathbf{k}'}\hat{c}_{\mu'\sigma',m'\mathbf{k}'} + \langle\hat{c}^{\dagger}_{\mu'\sigma',n'\mathbf{k}'}\hat{c}_{\mu'\sigma',m'\mathbf{k}'}\rangle\hat{c}^{\dagger}_{\mu\sigma,n\mathbf{k}}\hat{c}_{\mu\sigma,m\mathbf{k}}\right) \end{aligned} \tag{21}$$

and the Fock term is:

$$\begin{aligned} H^{\text{intra}}_{F} =& -\frac{1}{2N_s}\sum_{\mathbf{k}\mathbf{k}'}\sum_{\substack{\mu\mu'\\\sigma\sigma'}}\sum_{\substack{nm\\n'm'}}\left(\sum_{\mathbf{Q}} V(\mathbf{k}'-\mathbf{k}+\mathbf{Q})\Omega^{\mu\sigma,\mu'\sigma'}_{nm,n'm'}(\mathbf{k},\mathbf{k}',\mathbf{k}'-\mathbf{k},\mathbf{Q})\right) \\ &\times\left(\langle\hat{c}^{\dagger}_{\mu\sigma,n\mathbf{k}'}\hat{c}_{\mu'\sigma',m'\mathbf{k}'}\rangle\hat{c}^{\dagger}_{\mu'\sigma',n'\mathbf{k}}\hat{c}_{\mu\sigma,m\mathbf{k}} + \langle\hat{c}^{\dagger}_{\mu'\sigma',n'\mathbf{k}}\hat{c}_{\mu\sigma,m\mathbf{k}}\rangle\hat{c}^{\dagger}_{\mu\sigma,n\mathbf{k}'}\hat{c}_{\mu'\sigma',m'\mathbf{k}'}\right)\ . \end{aligned} \tag{22}$$

D. Constraint random phase approximation

We have taken screening effects caused by device into account. In this section, we consider further screening effects in band basis. To be specific, the interaction between electrons in flat bands can be screened by virtual excitation of particle-hole pairs from the remote bands. Such screening effects are evaluated by constrained random phase approximation(cRPA). We consider the bubble diagram for screened Coulomb interaction:

$$\begin{aligned} V^{cRPA}_{\mathbf{k}\mu nm,\mathbf{k}'\mu'm'n'}(\mathbf{q}) =& V^{0}_{\mathbf{k}\mu nm,\mathbf{k}'\mu'm'n'}(\mathbf{q}) \\ &+\frac{-2}{N_k}{\sum_{n_1m_1}}'\sum_{\mathbf{k}_1\mu_1} V^{0}_{k\mu nm,\mathbf{k}_1\mu_1m_1n_1}\chi^{0}_{\mathbf{k}_1\mu_1m_1n_1}(\mathbf{q})V^{0}_{\mathbf{k}_1\mu_1m_1n_1,\mathbf{k}'\mu'n'm'} \\ &+\left(\frac{-2}{N_s}\right)^2{\sum_{\substack{n_1m_1\\n_2m_2}}}'\sum_{\mu_1\mu_2}\sum_{\mathbf{k}_1\mathbf{k}_2} V^{0}_{\mathbf{k}\mu nm,\mathbf{k}_1\mu_1m_1n_1}\chi^{0}_{\mathbf{k}_1\mu_1m_1n_1}(\mathbf{q})V^{0}_{\mathbf{k}_1\mu_1m_1n_1,\mathbf{k}_2\mu_2m_2n_2}\chi^{0}_{\mathbf{k}_2\mu_2m_2n_2}(\mathbf{q})V^{0}_{\mathbf{k}_2\mu_2m_2n_2,\mathbf{k}'\mu'n'm'} \\ &+\dots \end{aligned} \tag{23}$$

We can define the single-gate screened Coulomb interaction projected to flat bands subspace:

$$V^{0}_{\mathbf{k}\mu nm,\mathbf{k}'\mu'm'n'}(\mathbf{q}) = \sum_{\mathbf{Q}} V(\mathbf{q}+\mathbf{Q})\lambda_{\mathbf{k}\mu nm}(\mathbf{q},\mathbf{Q})\lambda^{*}_{\mathbf{k}'\mu'm'n'}(\mathbf{q},\mathbf{Q}) \tag{24}$$

$$\lambda_{\mathbf{k}\mu nm}(\mathbf{q},\mathbf{Q}) = \sum_{\alpha\mathbf{G}} C^{*}_{\mu\alpha\mathbf{G}+\mathbf{Q},n}(\mathbf{k}+\mathbf{q})C_{\mu\alpha\mathbf{G},m}(\mathbf{k}) \tag{25}$$

where $\mathbf{G}$ is the moiré reciprocal lattice vector. The summation of band indices in Eq. (24) is restricted: m_1 and n_1 can not both come from the flat bands subspace. The remote bands below the flat bands are filled, while remote bands above the flat bands are empty. That is to say, the virtual excitation can happen through three channel: from the remote bands below the CNP to flat bands; from flat bands to the remote bands above CNP; from remote bands

below CNP to flat bands above CNP. We can define the bare susceptibility in the transferred reciprocal vectors basis $\chi^0_{Q,Q'}$ as:

$$\chi^0_{\mathbf{Q},\mathbf{Q}'} = \frac{2}{N_\mathbf{k}} \sum_{\mathbf{k}_1} {\sum_{\mu_1 m_1 n_1}}' \lambda^\dagger(\mathbf{q},\mathbf{Q})_{\mathbf{k}_1\mu_1 m_1 n_1} \chi^0_{\mathbf{k}_1\mu_1 m_1 n_1}(\mathbf{q}) \lambda(\mathbf{q},\mathbf{Q}')_{\mathbf{k}_1\mu_1 m_1 n_1} \tag{26}$$

where:

$$\chi^0_{\mathbf{k},\mu,m,n}(\mathbf{q},\nu) = \frac{f(E_{\mu,m,\mathbf{k}+\mathbf{q}}) - f(E_{\mu,n,\mathbf{k}})}{E_{\mu,n,\mathbf{k}} + \nu - E_{\mu,m,\mathbf{k}+\mathbf{q}}} \tag{27}$$

where μ is valley, $\mathbf{k}$ is wave vector in moiré Brillouin zone, m and n are band indices. Here we only consider static susceptibility, i.e. $\nu = 0$. We can rewrite the screened Coulomb interaction in matrix form:

$$\begin{aligned} \hat{V}^{cRPA}(\mathbf{q}) &= \hat{V}(\mathbf{q})_{\mathbf{Q},\mathbf{Q}} \delta_{\mathbf{Q},\mathbf{Q}'} \\ &+ \hat{V}(\mathbf{q})_{\mathbf{Q}\mathbf{Q}} (-\chi^0_{\mathbf{Q},\mathbf{Q}'}) \hat{V}(\mathbf{q})_{\mathbf{Q}'\mathbf{Q}'} \\ &+ \sum_{\mathbf{Q}''} \hat{V}(\mathbf{q})_{\mathbf{Q},\mathbf{Q}} (-\chi^0_{\mathbf{Q},\mathbf{Q}''}) \hat{V}(\mathbf{q})_{\mathbf{Q}'',\mathbf{Q}''} (-\chi^0_{\mathbf{Q}'',\mathbf{Q}'}) \hat{V}(\mathbf{q})_{\mathbf{Q}',\mathbf{Q}'} \\ &+ \dots \end{aligned} \tag{28}$$

$$= \hat{V}^0(\mathbf{q}) \cdot (\mathbb{1} + \chi^0(\mathbf{q}) \cdot \hat{V}^0(\mathbf{q}))^{-1} \tag{29}$$

We define the dielectric matrix as:

$$\hat{\epsilon}^{cRPA}(\mathbf{q})_{\mathbf{Q},\mathbf{Q}'} = (\mathbb{1} + \chi^0(\mathbf{q}) \cdot V^0(\mathbf{q}))_{\mathbf{Q},\mathbf{Q}'} \tag{30}$$

We can make Hartree-Fock approximation to the screened Coulomb interaction and decomposed into two terms. For the Hartree term, we take $\hat{V}^{cRPA}(\mathbf{q}=0)$, while we take $V(\mathbf{k}'-\mathbf{k}+\mathbf{Q})/\epsilon(\mathbf{k}'-\mathbf{k}+\mathbf{Q})$ for the Fock term.

E. Effects of lattice relaxations and non-identical twist angles

For moiré graphene systems with small twist angles, the low energy properties are sensitive to the lattice distortions. In the main text, we have considered the rigid moiré graphene layers with only out-of-plane corrugations, and the corrugation effects are manifested as the different inter-sublattice and intra-sublattice interlayer coupling parameters as discussed near Eq. (6) in Sec. I. In this section, we perform the lattice relaxation calculations for the A-ABA-A system and evaluate the relaxation effects on the band structures.

We can generalize the elastic model of TBG [6] to the ATMG systems. To be specific, we can express the intralayer elastic energy U_E and the interlayer binding energy U_B as a functional of the in-plane lattice displacement vectors:

$$\begin{aligned} U_E &= \sum_{l=1}^{5} \int \frac{1}{2} \{(\lambda+\mu)(u^{(l)}_{xx}(\mathbf{r}) + u^{(l)}_{yy}(\mathbf{r}))^2 + \mu[(u^{(l)}_{xx}(\mathbf{r}) - u^{(l)}_{yy}(\mathbf{r}))^2 + 4(u^{(l)}_{xy}(\mathbf{r}))^2]\} d^2\mathbf{r} \\ U_B &= \sum_{l=1}^{4} \int V[\boldsymbol{\delta}^{(l)}(\mathbf{r})] d^2\mathbf{r}, \end{aligned} \tag{31}$$

where $\{\mathbf{u}^{(l)}(\mathbf{r})$ (with $l = 1,\dots,5$) denotes the in-plane displacement vector of layer l at position $\mathbf{r}$, $\boldsymbol{\delta}^{(l)}(\mathbf{r})$ is the interlayer atomic shift vector between the lth layer and the $(l+1)$th layer at position $\mathbf{r}$, $\lambda \approx 3.5 eV\text{Å}^{-2}$ and $\mu \approx 7.8 eV\text{Å}^{-2}$, and $u^{(l)}_{ij}(\mathbf{r}) = (\partial_{r_i} u^{(l)}(\mathbf{r})_j + \partial_{r_j} u^{(l)}_i(\mathbf{r}))/2$ is the strain tensor at $\mathbf{r}$. The layer dependent binding energy

density is given by:

$$
\begin{aligned}
V^{(1)}[\boldsymbol{\delta}((r))] &= \sum_{j=1}^{3} 2V_0 \cos[\mathbf{G}_j^M \cdot \mathbf{r} + a_j^*(\mathbf{u}^{(2)} - \mathbf{u}^{(1)})], \\
V^{(2)}[\boldsymbol{\delta}((r))] &= \sum_{j=1}^{3} 2V_0 \cos[\frac{2\pi}{3} + a_j^*(\mathbf{u}^{(3)} - \mathbf{u}^{(2)})], \\
V^{(3)}[\boldsymbol{\delta}((r))] &= \sum_{j=1}^{3} 2V_0 \cos[-\frac{2\pi}{3} + a_j^*(\mathbf{u}^{(4)} - \mathbf{u}^{31)})], \\
V^{(4)}[\boldsymbol{\delta}((r))] &= \sum_{j=1}^{3} 2V_0 \cos[-\mathbf{G}_j^M \cdot \mathbf{r} + a_j^*(\mathbf{u}^{(5)} - \mathbf{u}^{(4)})],
\end{aligned}
\tag{32}
$$

where $\{\mathbf{G}_j^M, j = 1, 2, 3\}$ are the three primitive moiré reciprocal vectors, and $\{a_j^*, j = 1, 2, 3\}$ are the primitive reciprocal lattice vectors of the atomic graphene lattice. The total energy can be expressed as a functional of $\{\mathbf{u}^{(l,l+1)} = \mathbf{u}^{(l+1)} - \mathbf{u}^{(l)}\}$ $(l = 1, \ldots, 4)$ and $\{\mathbf{u}^{+}(\mathbf{r}) = \sum_{l=1}^{5} \mathbf{u}^{(l)}(\mathbf{r})\}$.

We can optimize the total energy by solving the Euler-Lagrange equation. Making use of the translational symmetry of the moiré supercell, we can perform Fourier transformation to various quantities related to the displacement vectors:

$$
\begin{aligned}
&\mathbf{u}^{(l,l+1)}(\mathbf{r}) = \sum_{\mathbf{q}} \mathbf{u}_q^{(l,l+1)} e^{i\mathbf{q}\cdot\mathbf{r}}, l = 1, \ldots, 4 \\
&\sin[\mathbf{G}_j^M \cdot \mathbf{r} + \mathbf{a}_j^* \cdot \mathbf{u}^{(1,2)}(\mathbf{r})] = \sum_{\mathbf{q}} f_{\mathbf{q}} e^{i\mathbf{q}\cdot\mathbf{r}}, \\
&\sin[\frac{2\pi}{3} + \mathbf{a}_j^* \cdot \mathbf{u}^{(2,3)}(\mathbf{r})] = \sum_{\mathbf{q}} g_{\mathbf{q}} e^{i\mathbf{q}\cdot\mathbf{r}}, \\
&\sin[-\frac{2\pi}{3} + \mathbf{a}_j^* \cdot \mathbf{u}^{(3,4)}(\mathbf{r})] = \sum_{\mathbf{q}} \bar{g}_{\mathbf{q}} e^{i\mathbf{q}\cdot\mathbf{r}}, \\
&\sin[\mathbf{G}_j^M \cdot \mathbf{r} + \mathbf{a}_j^* \cdot \mathbf{u}^{(4,5)}(\mathbf{r})] = \sum_{\mathbf{q}} \bar{f}_{\mathbf{q}} e^{i\mathbf{q}\cdot\mathbf{r}}.
\end{aligned}
\tag{33}
$$

where $\mathbf{q}$ denotes an arbitrary moiré reciprocal vector. Moreover, according to the mirror symmetry of the A-ABA-A system, $f_{\mathbf{q}}$, $\bar{f}_{\mathbf{q}}$, $g_{\mathbf{q}}$, and $\bar{g}_{\mathbf{q}}$ should satisfy the relationship, $f_{\mathbf{q}} = -\bar{f}_{\mathbf{q}}$, $g_{\mathbf{q}} = -\bar{g}_{\mathbf{q}}$. With the above considerations, the above Euler-Lagrange equation can be written in a succinct matrix form,

$$
\begin{aligned}
&\frac{1}{5} \cdot \begin{pmatrix} 4 & 3 & 2 & 1 \\ 3 & 6 & 4 & 2 \\ 2 & 4 & 6 & 3 \\ 1 & 2 & 3 & 4 \end{pmatrix} \otimes \hat{K}_{\mathbf{q}} = \hat{F}_{\mathbf{q}}, \\
&\text{where } \hat{K}_{\mathbf{q}} = \begin{pmatrix} (\lambda + 2\mu)q_x^2 + \mu q_y^2 & (\lambda + \mu)q_x q_y \\ (\lambda + \mu)q_x q_y & (\lambda + 2\mu)q_y^2 + \mu q_x^2 \end{pmatrix}, \\
&\hat{F}_{\mathbf{q}}^{\mathrm{T}} = \left(a_{j,x}^* f_{q_x}^j, a_{j,y}^* f_{q_y}^j, a_{j,x}^* g_{q_x}^j, \ldots, a_{j,x}^* \bar{f}_{q_x}^j, a_{j,y}^* \bar{f}_{q_y}^j\right)
\end{aligned}
\tag{34}
$$

We can numerically find the self-consistent solutions of the above Euler-Lagrange equation for the A-ABA-A system. In Supplementary Figure. 1(a) and (c), we show the real-space distributions of the in-plane displacement vectors (with respect to the ideal moiré superlattice) for each layer of the A-ABA-A ATMG system in the fully relaxed structure at $\theta = 1.121\,^\circ$ and $\theta = 0.906\,^\circ$ respectively, where the color coding represents the amplitudes of the in-plane displacement vectors. We see that for both angles, the lattice deformations are strongest in the very top and very bottom layers, which give rise to expanded AB/BA regions and contracted AA regions, similar to the relaxation pattern of twisted bilayer graphene. The deformations are weaker in the second and fourth layers, and is weakest in the middle layer. This is because the middle layer forms an atomistic Bernal stacking with the second and fourth layers, which has a strong binding energy and is hard to deviate from the equilibrium position. Further analysis reveals that the in-plane displacement vectors of the first and second layers (as well as those of the fourth and fifth layers) also wind around their AA point, forming a vortex-like vector field surrounding the AA point, which is also similar to the relaxation pattern in magic-angle twisted bilayer graphene [7, 8].

Then we generalize the continuum model for twisted bilayer graphene including the effects of lattice deformations [6] to ATMG system. For small twist angle and slowly varying displacement vectors, the interlayer hopping matrix element between the Bloch states from two twisted layers can be expressed as:

$$\begin{aligned}
&\langle \mathbf{k}', \mathbf{X}', 2| \, U \, |\mathbf{k}, \mathbf{X}, 1\rangle = \frac{1}{S} \int d^2 r e^{i(\mathbf{k}-\mathbf{k}')\cdot \mathbf{r}} U_{X'X} \ , \\
&\text{where} \ \ U^{1,2}_{X'X}(\mathbf{r}) = -\sum_{j=1}^{3} M^{j}_{X'X} \, t_{\parallel}[\mathbf{Q}_j; d_0 + u_z^{(1,2)}(\mathbf{r})] \, e^{i(\mathbf{Q}_j \cdot \mathbf{u}_{\mathbf{r}}^{(1,2)} + \delta \mathbf{k}_j \cdot \mathbf{r})} \ , \\
&\text{and} \ \ \langle \mathbf{k}', \mathbf{X}', 4| \, U \, |\mathbf{k}, \mathbf{X}, 5\rangle = \frac{1}{S} \int d^2 r \, e^{i(\mathbf{k}-\mathbf{k}')\cdot \mathbf{r}} \, U^{4,5}_{X'X} \ , \\
&\text{where} \ \ U^{45}_{X'X}(\mathbf{r}) = -\sum_{j=1}^{3} M^{j}_{X'X} t_{\parallel}[\mathbf{Q}_j; d_0 + u_z^{(4,5)}(\mathbf{r})] \, e^{i(\mathbf{Q}_j \cdot \mathbf{u}_{\mathbf{r}}^{(4,5)} + \delta \mathbf{k}_j \cdot \mathbf{r})}.
\end{aligned} \tag{35}$$

On the other hand, the lattice deformation couples to the intralayer component of the electronic Hamiltonian as a pesudovector potential:

$$H_l(\mathbf{k}) = -\hbar v_F [\mathbf{k} + \frac{e}{\hbar} \mathbf{A}^{(l)} - \mathbf{K}^{(l)}] \cdot \boldsymbol{\sigma}^{\mu} \ , \tag{36}$$

where

$$\mathbf{A}^{(l)} = \xi \frac{3}{4} \frac{\beta \gamma_0}{ev} \sigma_{\mathbf{q}} \hat{W}_{\mathbf{q}} \mathbf{u}^{(l)}_{\mathbf{q}} e^{i\mathbf{q}\cdot\mathbf{r}} \ , \tag{37}$$

and

$$\hat{W}_{\mathbf{q}} = \begin{pmatrix} iq_x & -iq_y \\ -iq_y & -iq_x. \end{pmatrix} \tag{38}$$

In Supplementary Figure. 1(b) and (d) we provide the band structures for relaxed A-ABA-A system at different twist angles. Depending on twist angles, structural relaxations may either enhance or reduce the bandwidth of the double flat bands. For example, for $\theta = 1.121$, the lattice deformation would significantly enhance the bandwidth as shown in Supplementary Figure. 1(b). As a result, the double flat bands would be entangled with the remote bands. For $\theta = 0.906$, the lattice deformation would reduce the bandwidth of the double flat bands as shown in Supplementary Figure. 1(b), which have a total bandwidth $\sim$ 25meV, and are separated from the remote energy bands by a gap $\sim 10\,$meV. We also check that the total valley Chern number of these flat bands are unchanged after including the structural relaxation effects. Flatter double flat bands imply stronger interacting effects. Therefore, we conclude that the orbital magnetoelectric effect, which is a result of strong correlations of the topological flat bands in mirror-symmetric ATMG system, would remain robust even including the structural relaxation effects.

We have also considered the effects of non-identical twist angles by changing one of the two twist angles by $P = \delta\theta/\theta = 5\%$, and the Dirac point of one of the three multilayer sequences is shifted by $\delta\mathbf{K}$ accordingly. Then the intralayer Hamiltonian for one of the three multilayer sequences is changed by:

$$\delta H = \hbar v_F \delta \mathbf{K} \cdot \boldsymbol{\sigma}^{\mu} \tag{39}$$

In Supplementary Figure. 2(a) we show the band structures of A-ABA-A ATMG system with exactly opposite twist angles ($P = 0$), and in Supplementary Figure. 2(b) we show the band structures of the same system with one of the twist angles changed by 5% ($P = 5\%$). We see that the two band structures are nearly identical. Thus, we conclude that the inequivalent twist angles would have very weak effects on the low-energy electronic structures, and does not change the conclusion of our work.

II. SUPPLEMENTARY FIGURES

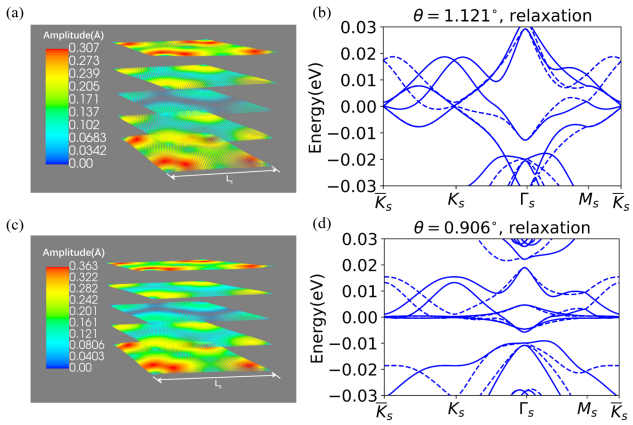

Supplementary Figure. 1: Lattice relaxations and band structures with relaxed lattice structures. The real-space distribution of the in-plane displacement vectors for each layer of the A-ABA-A system: (a) at $\theta = 1.121°$, and (c) at $\theta = 0.906°$. The color coding represents the amplitudes of the displacements, in units of angstroms. The band structures of the A-ABA-A ATMG system including the structural relaxation effects: (b) at $\theta = 1.121°$, and (d) at $\theta = 0.906°$.

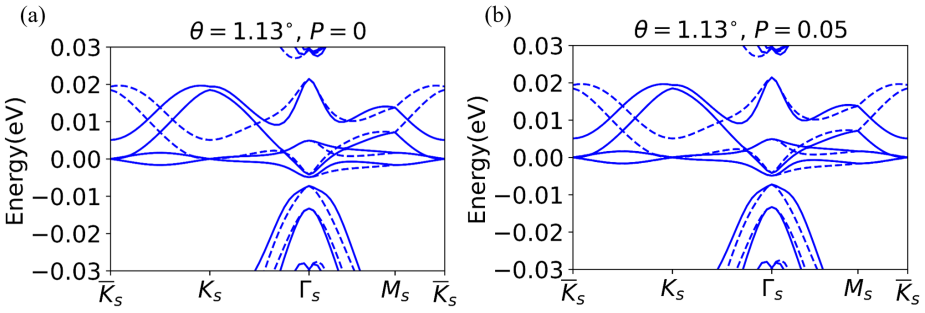

Supplementary Figure. 2: The band structure of the A-ABA-A ATMG system at $\theta = 1.13°$, (a) with identical twist angles, and (b) with one of the twist angles changed by 5%.

III. SUPPLEMENTARY REFERENCES

[1] Bistritzer, R. & MacDonald, A. H. Moiré bands in twisted double-layer graphene. Proceedings of the National Academy of Sciences **108**, 12233–12237 (2011).

[2] Liu, J., Ma, Z., Gao, J. & Dai, X. Quantum valley hall effect, orbital magnetism, and anomalous hall effect in twisted multilayer graphene systems. Phys. Rev. X **9**, 031021 (2019).

[3] Koshino, M. et al. Maximally localized wannier orbitals and the extended hubbard model for twisted bilayer graphene. Phys. Rev. X **8**, 031087 (2018).

[4] Tarnopolsky, G., Kruchkov, A. J. & Vishwanath, A. Origin of magic angles in twisted bilayer graphene. Phys. Rev. Lett. **122**, 106405 (2019).

[5] Lee, J. Y. et al. Theory of correlated insulating behaviour and spin-triplet superconductivity in twisted double bilayer graphene. Nature Communications **10**, 5333 (2019).

[6] Koshino, M. & Son, Y.-W. Moiré phonons in twisted bilayer graphene. Phys. Rev. B **100**, 075416 (2019).

[7] Cantele, G. et al. Structural relaxation and low-energy properties of twisted bilayer graphene. Phys. Rev. Research **2**, 043127 (2020).

[8] Liu, X., Peng, R., Sun, Z. & Liu, J. Phonons in magic-angle twisted bilayer graphene. arXiv Preprint at arXiv: 2112.13240 (2021).